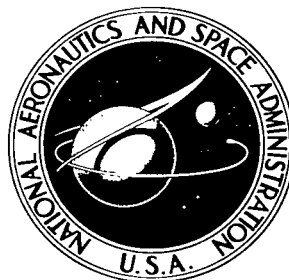


NASA TECHNICAL NOTE



NASA TN D-3425

NASA TN D-3425

LOAN COPY: RI
AFWL (WI
KIRTLAND AFB

0130168



TECH LIBRARY KAFB, NM

ACOUSTIC DECAY COEFFICIENTS OF SIMULATED ROCKET COMBUSTORS

by Paul R. Wieber
Lewis Research Center
Cleveland, Ohio





ACOUSTIC DECAY COEFFICIENTS OF SIMULATED ROCKET COMBUSTORS

By Paul R. Wieber

Lewis Research Center
Cleveland, Ohio

NATIONAL AERONAUTICS AND SPACE ADMINISTRATION

For sale by the Clearinghouse for Federal Scientific and Technical Information
Springfield, Virginia 22151 - Price \$1.00

ACOUSTIC DECAY COEFFICIENTS OF SIMULATED ROCKET COMBUSTORS

by Paul R. Wieber

Lewis Research Center

SUMMARY

Cold acoustic bench tests were made to obtain coefficients of decay of cylindrical acoustic modes in simulated rocket combustion chambers with no throughflow. The tests were performed to obtain decay coefficients for typical chambers with and without baffles and to indicate damping trends with chamber length, nozzle angle, and injector and baffle shapes.

The tests were made by generating the desired mode with an acoustic driver in the simulated combustor at atmospheric pressure. When the power to the driver was abruptly shut off, the decay of the field was monitored with wall-mounted condenser microphones. All tests were run at acoustic pressure levels of 123 to 143 decibels (0.0041 to 0.041 psi, 28 to 280 N/m²); so the acoustic field was essentially sinusoidal in behavior. The nozzle was plugged at the throat.

The results for unbaffled chambers showed that the damping of the fundamental standing transverse mode increased with increasing internal area-to-volume ratio of the test chamber. The effective acoustic length of the chambers was determined from the resonant frequency of the longitudinal mode, and the decay per cycle of this mode increased with increasing effective length. The effective length of tapered chambers depended on injector shape and was a function of nozzle convergence angle. Pure radial modes usually could not be generated in noncylindrical chambers but exhibited low damping per cycle compared to the other two fundamental modes.

Baffle shapes comprising radial vanes and circular rings distorted the acoustic fields by obstructing particle motion and usually produced much higher damping than unbaffled chambers. Data for baffled chambers are included, but no correlation for the baffles was found.

INTRODUCTION

The high-frequency pressure and particle-velocity oscillations which occur in liquid-

and solid-propellant rocket engines are often identifiable with the cylindrical acoustic modes of the combustion chamber. These combustion-driven waves produce heat-transfer rates and vibration levels which are destructive to engine hardware. Therefore, a successful combustor design must show no incidence of combustion instability. For this reason, investigations such as those of references 1 to 3 have been made to determine the processes which could affect wave growth and decay during combustor operation. They indicate the existence of stable and unstable operating zones.

Recent reports have contained work in which the acoustic aspects of the combustor are emphasized. In reference 4 the combustion process was approximated by simplifying assumptions in order to determine analytically the effect of nozzle shape and position on the acoustic power radiated through the nozzle. The same topic was experimentally studied and reported in reference 5, a purely acoustical study which related flow-dependent nozzle losses to vent-flow Mach number and vent position.

Mechanical devices such as baffles and liners are potential dampers for acoustic combustion instability. It was shown in reference 6 that the proper placement of baffles in a previously unstable rocket engine can stabilize the combustion. A recent analysis (ref. 7) attempted to establish a theoretical basis for baffle design for the transverse acoustic mode. Chamber damping can also be appreciably increased by the use of perforated acoustic liners, as shown in reference 8.

The evaluation of acoustic decay coefficients of complex cavities is not amenable to theoretical analyses because such analyses usually necessitate a simplified coordinate system and/or boundary conditions. Many acoustic experiments have been reported which involved the determination of the damping properties of simple geometrically shaped chambers. However, such data usually cannot be extrapolated to cavities comprised of combinations of simple shapes. Studies have not been reported on the damping characteristics of combinations of various geometric shapes, both baffled and unbaffled, which might be suitable for rocket combustors.

This report presents experimental values and trends for acoustic decay coefficients in simulated rocket chambers with no throughflow. The investigation is concerned with the effect of nozzle convergence angle, chamber length, injector shape, and insertion of baffles on the damping properties of normally cylindrical chambers. Most configurations studied had nozzle shapes and length-to-diameter ratios typical of commercial combustors. The diameter of the injector end of the chamber was held at 6 inches (15.24 cm), while total chamber length, measured from the nozzle throat to the top of the chamber walls and therefore independent of injector shape, was varied from 4 to 12 inches (10.16 to 30.48 cm). The nozzle convergence angle was varied from 180° (perpendicular to the chamber axis) to a minimum of 20° . Four cylindrically symmetrical injector shapes and several baffle patterns of 3-inch-long (7.62-cm) fins and posts were tested.

All tests were run with the chamber filled with dry nitrogen at ambient conditions

(1 atm, 20° C). Steady-state acoustic sound pressure levels ranged between 123 and 143 decibels (referenced to 2×10^{-5} N/m²), values equivalent to root-mean-square pressures between 0.0041 and 0.041 pound per square inch (28 and 280 N/m²). Damping coefficients were obtained by monitoring the exponential decay of the acoustic modes in the chamber after driving ceased. The results are related to the chamber internal area-to-volume ratio and to acoustic resonating length. Baffle results are tabulated.

THEORY

The measurement of the decay of sound in chambers was first used in studies of architectural acoustics made during the early part of this century, such as reference 9. Both the earlier and later studies on this subject are abundant with such measurements. Upon initiation of an acoustic source, the sound level in the chamber rose exponentially to an intensity level I_0 where the losses due to damping equaled the driving energy. Shutting off the source caused the sound intensity I to decay again exponentially with time so that

$$I = I_0 e^{-K_I t} \quad (1)$$

where t is time and K_I , the fractional loss per second, was found to be

$$K_I = \frac{ac}{4} \frac{A}{V} \quad (2)$$

In equation (2) a is the absorption coefficient of the wall material of uniform composition, c is the velocity of sound, and A and V are the internal surface area and the internal volume of the chamber, respectively. Equation (2) is valid for a diffuse or "white noise" sound field, where all unit areas of surface are exposed to the same acoustic energy density.

In contrast, acoustic combustion instability is identifiable with ordered sound fields where one frequency predominates and pressure and particle fluctuations are both periodic with time and dependent upon spatial position within the chamber. If the damping effects are first order in this type of acoustic field, the decay of the energy envelope will be described by an exponential equation similar to equation (1). However, since the energy density of an ordered field shows spatial variation throughout the resonant volume, the energy losses are also not equal for each unit area, and the functional dependency of the exponential decay coefficient is not necessarily given by equation (2).

In the present study, damping factors such as wave interaction due to geometric distortion, viscous gas losses, and viscous boundary-layer losses affect the coefficient of decay. It is assumed that acoustic admittance at the wall has a minor effect. This assumption is supported by figure 12 of reference 10, which shows that all wall mechanical losses contributed only about 4 percent to the total absorption in a tube with a 0.255-inch (0.648-cm) wall thickness.

It is more convenient to measure sound pressure P rather than energy. This was done in the present work. The equation used was

$$P = P_0 e^{-K_P t} \quad (3)$$

where P_0 is the steady-state sound pressure before decay, and K_P is the decay rate.

The damping coefficient is reported herein as the fractional pressure loss per cycle obtained by dividing the exponential decay rate by the resonant frequency:

$$K' = \frac{K_P}{f} \quad (4)$$

This number can be converted to pressure level loss in decibels per cycle by multiplying by 8.686. Since the wave energy is proportional to the square of the pressure, K' can be converted to fractional energy loss per cycle by multiplying by 2.

The frequencies of the possible cylindrical modes are given by the following equation:

$$f = \frac{c}{2} \sqrt{\left(\frac{\alpha_{m,n}}{R}\right)^2 + \left(\frac{n_z}{L}\right)^2} \quad (5)$$

where f is the frequency in cps, c is the speed of sound in feet per second, $\alpha_{m,n}$ is a constant which depends on the transverse mode number m and on the radial mode number n , R is the chamber radius in feet, n_z is the longitudinal mode number, and L is the chamber length in feet. A table of values for $\alpha_{m,n}$ is given in reference 11. Resonant frequencies for cylinders with dimensions similar to the test configurations were calculated from equation (5) and were used to locate approximately the acoustic modes in the frequency spectrum in the test chambers. (The maximum radius was used for the tapered chambers.)

APPARATUS AND PROCEDURE

The acoustic field was produced by a variable-frequency audio oscillator energizing a 25-watt loudspeaker driver mounted on the test chamber. The driving system was operated in a voltage range which ensured a sinusoidal output with a minimum of distortion. The decay was initiated by a nonchattering switch which simultaneously disconnected the audio oscillator from the driver, shorted across the driver to resist further diaphragm motion, and shunted the driving signal to another reactance to protect the audio oscillator. It was found that a single driver could generate most pure and combination acoustic modes in cylindrical chambers except the traveling transverse modes.

The test chambers were made from a number of interchangeable aluminum sections as shown in figure 1. The sections were stepped so that they would interlock and their inner walls would be accurately aligned. The first segment below the simulated injector was common to all the configurations and held the acoustic driver and primary microphone. A variable number of cylindrical chamber segments were located below the instrumented section, and these were followed by an exhaust nozzle section. The nozzle section was smoothed at the chamber wall by a radius of 0.5 inch (1.27 cm). The nozzle throat diameter was $2\frac{3}{8}$ inches (6.03 cm). Since only internal chamber damping was to be studied, the nozzle throat was blocked by a flat plate to prohibit acoustic losses through

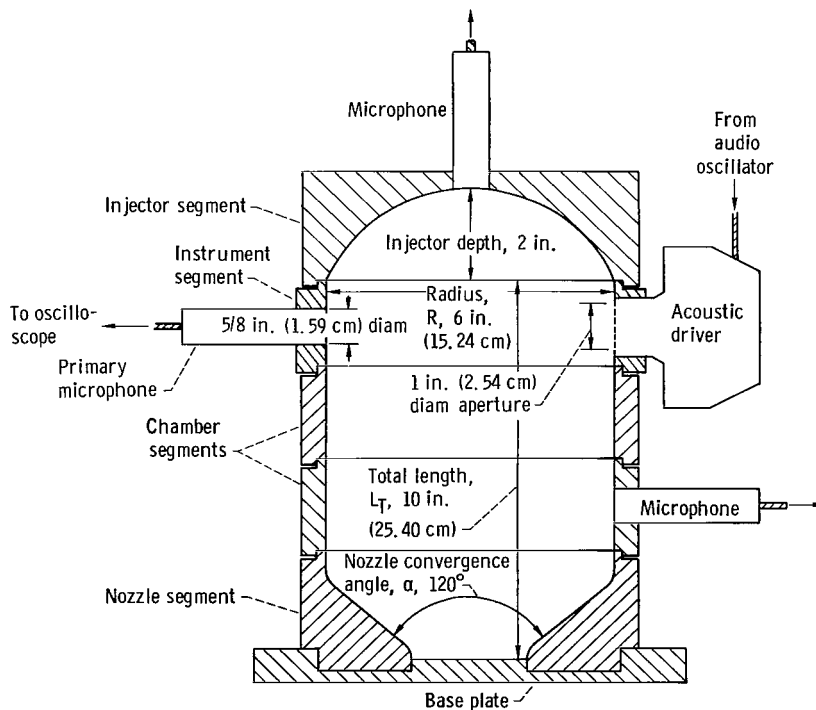


Figure 1. - Simulated rocket chamber for acoustic tests. Total length varies from 4 to 12 inches (10.16 to 30.48 cm); nozzle convergence angle varies from 20° to 180°.

the nozzle. For maximum chamber taper (minimum convergence angle), the nozzle segment comprised the entire chamber below the instrument segment.

The acoustic field was monitored by three flush-mounted type 21 BR 150 condenser microphones with associated self-regulating power supplies. These microphones have a usable frequency range of 5 to 15 000 cps. The diameters of the microphones and driver were 0.625 and 1.0 inch (1.59 and 2.54 cm), respectively. The decay measurements were made with the primary microphone opposite the driver in the instrument segment. A pressure antinode always occurred at this location for all modes studied. The secondary microphones could be moved around the chamber and over the injector face and the nozzle walls for the purpose of verifying which acoustic mode was present in the chamber by means of phase and amplitude comparisons of output signals.

For decay measurements the driver input and the primary microphone output were displayed on a chopped dual-beam oscilloscope. A 1000-cps pulse generator was connected to one of the chopped beams for an accurate time base. The oscilloscope screen was photographed with a variable-speed 16-mm streak camera.

At the start of a series of tests, the test chamber was purged with dry nitrogen. Next, the desired acoustic mode was generated by setting the driver frequency at the calculated cylindrical resonant frequency and then adjusting the frequency slightly around this point until the output amplitude of the primary microphone reached a maximum. This was considered to be the true resonance point in the frequency range. The spatial phase relations of the mode were checked, and the camera was started. When the camera reached a relatively constant speed of about 5 to 10 feet per second, the loudspeaker driver was repeatedly turned off and on to record the acoustic field decay. A typical decay trace is shown in figure 2.

The film traces were analyzed on a reader. The data were treated by a digital computer program which obtained the exponential decay constant in equation (3) by a least-squares curve fit.

Decay measurements of the same acoustic mode and chamber configuration were repeated a number of times. From these runs the overall experimental error was found to be approximately ± 8 percent of the mean value. No significant variation in the damping coefficient with driver voltage was found.

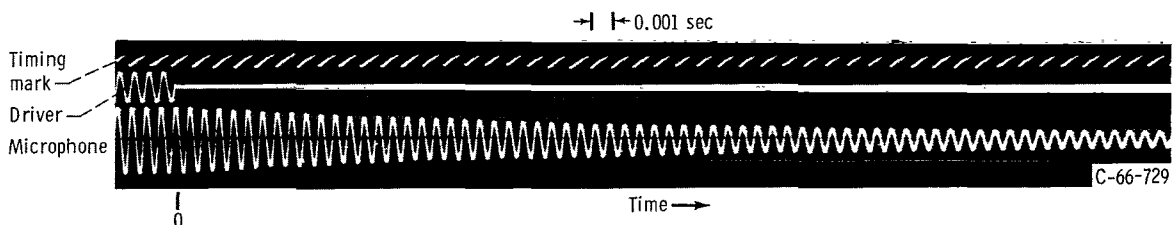


Figure 2. - Typical decay trace for first standing transverse mode. Chamber total length, 12 inches (30.48 cm); nozzle convergence angle, 20° ; flat injector configuration.

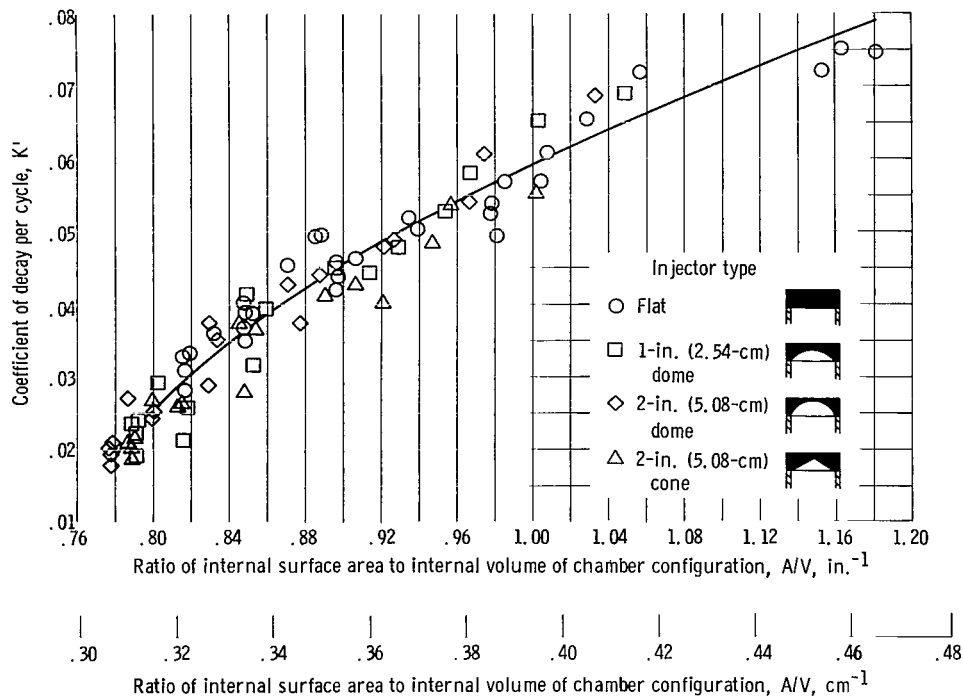


Figure 3. - Variation of first standing transverse mode decay coefficients with chamber surface-to-volume ratio.

RESULTS AND DISCUSSION

Unbaffled Chamber

Transverse mode. - The damping coefficients for diffuse sound fields have been shown by equation (2) to depend on the ratio of the internal surface area to the internal volume of the chamber. A dependency on this parameter was therefore investigated in the present study. The gas motion associated with the first standing transverse mode acts over the entire internal surface of the chamber. Figure 3 shows that the damping coefficient of this mode does correlate with the area-to-volume ratio for unbaffled, cylindrically symmetric chambers. The data include nozzle convergence angles from 20° to 180° and total lengths from 4 to 12 inches (10.16 to 30.48 cm) for the four injector shapes shown in figure 3. A few data with a nozzle angle of 34° were omitted because phase and amplitude measurements did not positively identify the acoustic mode in these configurations.

The dependency of the damping coefficient on the area-to-volume ratio implies that viscous dissipation of acoustic energy to the chamber walls provided the major loss for the mode. The acoustic field retained the characteristics of a pure cylindrical mode

since length and nozzle angle show no systematic effect on data spread. A value of zero for the area-to-volume ratio implies a chamber of zero area or infinite volume. Based on the idea of viscous dissipation losses as the sole important loss mechanism, there should be no damping for zero area-to-volume ratio. Extrapolation of the data does not give a (0, 0) intercept. Either the extrapolation is invalid, or the physical concept does not apply at low values of the area-to-volume ratio.

Longitudinal mode. - When the effective chamber area for the first standing longitudinal mode is calculated, the area of the ends of the chamber should probably be omitted since theoretically there is no gas motion at the ends. The end area for a tapered chamber is not clearly defined. However, the decay coefficient showed no relation to either total area-to-volume ratio or side area-to-volume ratio.

As the chambers were tapered with chamber total length held constant, the resonant frequency for the longitudinal mode was highest at the nozzle convergence angle of 34° . Substitution of the measured resonant frequency into equation (5) gave an equivalent acoustic resonant length. This is the length of a purely cylindrical chamber which would reso-

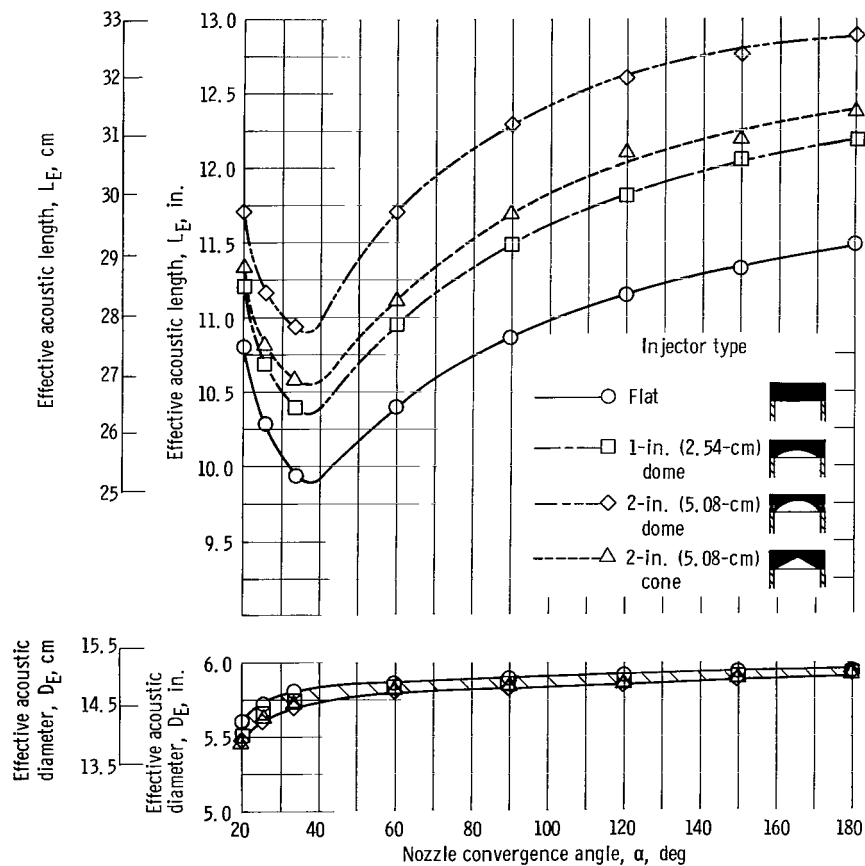


Figure 4. - Variation of effective acoustic length and diameter with nozzle convergence angle. Total length, 12 inches (30.48 cm); injector diameter, 6 inches (15.24 cm).

nate at the same frequency as the test chamber. The variation of the effective length with nozzle angle for four different injector shapes and a total length of 12 inches (30.48 cm) (with injector depth excluded) is shown in figure 4. Injector shape appears as an additive factor, moving the curve higher or lower without changing its shape. Resonant frequencies for the pure transverse mode were treated similarly to get an effective radius, also plotted in figure 4. Chambers with shorter total lengths showed similar characteristics.

The physical interpretation of figure 4 is that tapering the cylinder changes the wave reflection and gas particle motion at the nozzle end so that the chamber is at first acoustically shortened to the longitudinal mode. At a nozzle convergence angle of 180° most of the wave energy is reflected from the nozzle wall and relatively little from the nozzle plug. As the nozzle angle becomes smaller, the wave reflection toward the injector from the steepening nozzle walls becomes less efficient. However, the nozzle plug is flat and can still reflect acoustic energy effectively. At some nozzle convergence angle between 60° and 34° , the energy reflected from the nozzle plug equals that reflected from the nozzle walls. At smaller nozzle angles reflection from the nozzle plug predominates and the acoustic field resonates deeper in the nozzle and more toward the center of the combustor, as indicated by the increase in effective length and decrease in effective radius. The final limit at a nozzle convergence angle of 0° would be resonance in the cylindrical section between the nozzle plug and the injector face.

The effective length was the only parameter found which indicated the behavior of the longitudinal mode as the chamber was tapered. The decay coefficient can be correlated with the effective length.

Figure 5 shows the effect of nozzle convergence angle on the variation in damping coefficient with effective length for a flat injector. Other injector shapes gave similar trends. Total length varies from 4 to 12 inches (10.16 to 30.48 cm). The upper curve passes through data for nozzle angles greater than or equal to 60° , while the lower curve includes data for angles less than 60° . The 6-inch (15.24 cm) chamber data show the greatest spread. This configuration is "square"; that is, its length almost equals its diameter. Such systems are acoustically very complex because both the longitudinal and transverse modes resonate at about the same frequency and can interact with each other.

The increase of the decay coefficient with effective length supports the assumption that viscous dissipation to the side walls contributes significantly to longitudinal mode damping. The increase in damping is not linear with effective length as would be the case if an average loss per unit length of wall were the only controlling factor. Instead, the effect of nozzle shape on wave reflection must also come into play. This is consistent with the work of reference 12 involving flow, in which the nozzle resistance and phase shift of longitudinal waves in nozzles were found to be dependent on nozzle shape. A comparison of calculated nozzle impedance from reference 12 and the present work is not readily available because of the complexity of the theoretical equations and inability to

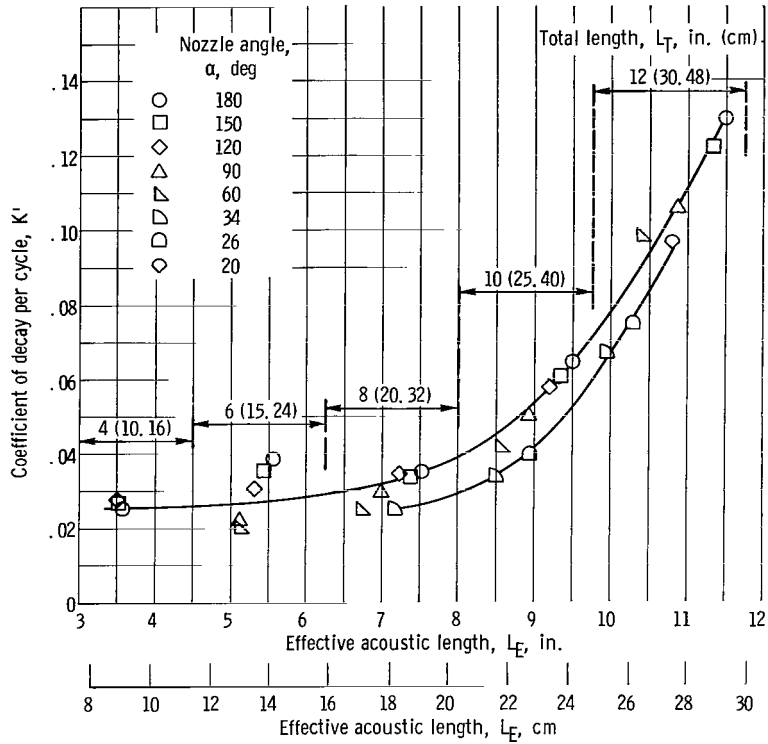


Figure 5. - Effect of nozzle convergence angle on variation of first standing longitudinal mode decay coefficients with effective acoustic length. Flat injector.

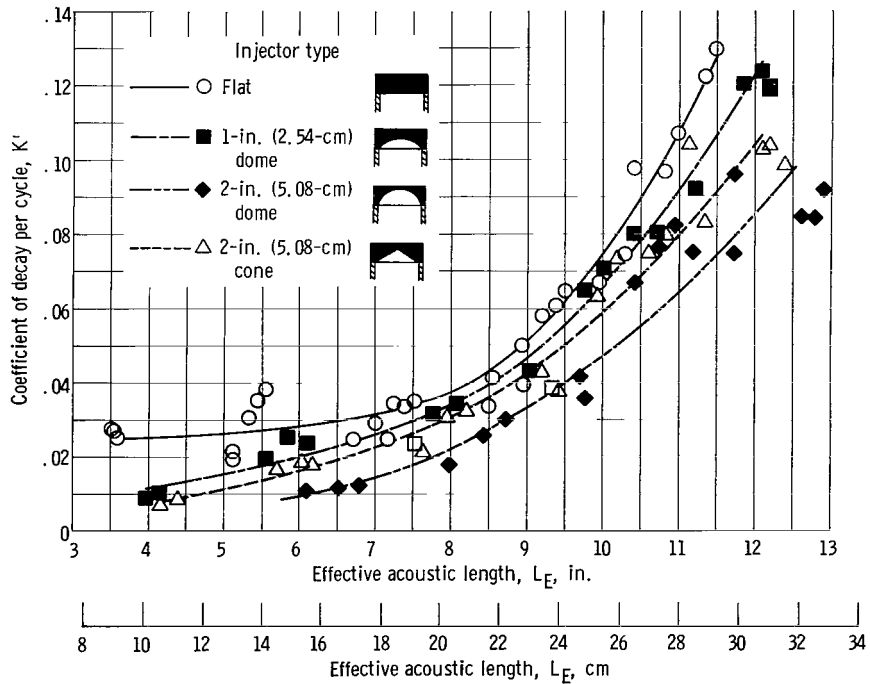


Figure 6. - Effect of injector shape on variation of first standing longitudinal mode decay coefficients with effective acoustic length.

solve them for many nozzle conditions. Figure 5 shows that purely cylindrical chambers gave the maximum chamber damping for a fixed total length. Two chamber configurations can have the same effective length, and the configuration with the lower nozzle angle gives less damping than the one with the higher nozzle angle for a given effective length. This damping characteristic may be due to the concentration of acoustic energy in the center of the tapered chambers and to the corresponding reduction of losses at the chamber walls.

Figure 6 shows the effect of injector shapes on the variation of the coefficient of decay with effective acoustic length. Each curve represents data for all nozzle angles from 20° to 180° . Different injector shapes show the same general damping trends, but the decay coefficients of dished configurations are lower than those for the flat injector. It would be expected that the injectors would behave acoustically the same as the nozzles for no throughflow. This would have given only one curve in figure 6 for all four injectors. The data show that the injector end of the chamber reacts differently from the nozzle end. This may be attributed to the presence of the driver in the injector end, which restricts the compliance of the acoustic field to a change in end shape.

Comparison of fundamental modes in unbaffled chambers. - Because of the nearness of many other combination modes, it was usually not possible to generate a pure radial mode. Thus, only a few radial decay measurements were made. Table I presents the data on the three fundamental modes for cylindrical configurations of lengths from 4 to 12 inches (10.16 to 30.48 cm). Comparison shows that the radial mode decayed much slower than either the transverse or longitudinal mode. This difference is reasonable

TABLE I. - COEFFICIENTS OF DECAY PER CYCLE AND RESONANT FREQUENCIES OF FUNDAMENTAL MODES

[Flat injector; nozzle angle, α , 180°]

Total length, L_T ,		Mode					
		Longitudinal		Transverse		Radial	
in.	cm	Coefficient of decay per cycle, K'	Resonant frequency, f , cps	Coefficient of decay per cycle, K'	Resonant frequency, f , cps	Coefficient of decay per cycle, K'	Resonant frequency, f , cps
12	30.48	0.1295	598	0.0304	1364	0.00564	2838
10	25.40	.0642	728	.0389	1360	.00963	2871
8	20.32	.0350	921	.0419	1362	.01165	2944
6	15.24	.0383	1241	.0524	1370	.00822	2794
4	10.16	.0252	1905	.0721	1389	.00880	2729

since ideally only the cylinder ends would experience gas motion with viscous losses for the radial modes.

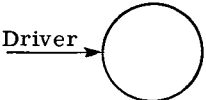
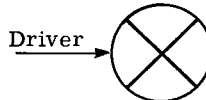
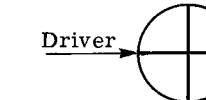
Equations were derived in reference 13 which gave the ratio of the rate of viscous dissipation of energy to the total wave energy, both averaged over one cycle of oscillation in a cylinder. Application of these equations to the 12-inch (30.48-cm) chamber gave longitudinal and transverse mode damping coefficients about 15 times lower than the experimental values. However, both the experimental and theoretical data gave a decay coefficient for the longitudinal mode which is roughly four times that for the transverse mode. No losses were predicted for the radial mode, and the equations indicate no variation in transverse mode losses with chamber length. The experimental data only verify the calculated relative dissipation among the three fundamental modes in the 12-inch-long (30.48-cm) chamber.

Baffled Chambers

The insertion of mechanical damping devices such as baffles in the chamber can potentially increase acoustic decay rates. The orientation of the baffles with respect to the ordered acoustic field is important. Table II shows the pressure levels detected by the

TABLE II. - EFFECT OF BAFFLE ORIENTATION RELATIVE TO DRIVER
ON STEADY-STATE DAMPING OF TRANSVERSE MODES

[Total chamber length, L_T , 6.0 in. (15.24 cm); nozzle angle, α , 180° ; rms driver input voltage, 2.0 V; driver axial distance from injector face, 1 in. (2.54 cm).]

Transverse mode number, m	Configuration								
	1 (Flat injector)			2 (Flat injector with 3-in.-long (7.62-cm) radial vanes)			3 (Flat injector with 3-in.-long (7.62-cm) radial vanes)		
	Driver → 			Driver → 			Driver → 		
	Resonant frequency, f, cps	rms pressure level		Resonant frequency, f, cps	rms pressure level		Resonant frequency, f, cps	rms pressure level	
dB		psi	dB		psi	dB		psi	
1	1367	141.4	0.034	885	140.5	0.031	858	135.0	0.017
2	2257	143.1	.042	----	-----	-----	2300	141.0	.033
3	3095	140.0	.029	3080	140.0	.029	----	-----	-----

primary microphone when the driver, held at constant voltage, was inserted into an un-baffled chamber (configuration 1) and into two chambers with differently oriented baffled injectors (configurations 2 and 3). The driver and microphone were within the baffled sections of the chambers, 180° apart. Transverse modes of oscillation were generated. It is assumed that the amplitude of the pressure level gives an approximate measure of the chamber steady-state damping. The damping is due to both the orientation of the vanes and the angular driving location, since an acoustic field cannot be driven at a pressure node. For the transverse mode, the pressure antinode follows the driver; so the influence of driving location is minimal.

The two baffled chambers decrease the frequency and pressure level of the first transverse mode. The lowered frequency may correspond to an increased path length for the wave. Configuration 3 gave a considerably lower pressure level. The vane positioned at right angles to the driving line lies on a velocity antinode. It not only provides viscous damping but also blocks the gas particle motion. The same effect is apparent for the higher modes. The velocity antinode for the second transverse mode lies on both vanes in configuration 2, and this mode could not be obtained. Similarly, the third mode could not be obtained in configuration 3.

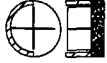
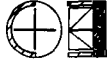
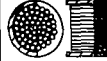
It was observed that, when the driver was shut off, the acoustic field rotated to an orientation giving the least damping within a few cycles and then decayed. For the fundamental transverse mode, configuration 2 provided the least damping, and all decays for chambers with radial vaned baffles were measured by using this driver-baffle orientation to avoid the angular rotation of the acoustic field.

Although baffles usually contributed appreciable damping, no distinct trends were observed. The data are therefore presented in tabular form in table III. The left column shows the front and side views of the baffle pattern used on the injector. The unbaffled injectors are included for comparison. Decay coefficients K' and associated resonant frequencies f for each configuration are shown in the table. No radial data were taken. Data are shown for total chamber lengths from 4 to 12 inches (10.16 to 30.48 cm) and nozzle convergence angles of 180° and 26° .

The vaned baffles had two patterns, one with two radial vanes at right angles and the other with the first pattern plus a 2-inch-diameter (5.08-cm) cylindrical ring. Vane and ring heights were 3 inches (7.62 cm). These two patterns were built on two injector types. The first type was a flat-face injector shown in the first, second, and third rows of table III. The second type was a cone which protruded into the chamber with an apex of 3 inches (7.62 cm), and it is shown in the fourth, fifth, and sixth rows of table III. The last three rows present data for baffles consisting of a random array of 3-inch-long (7.62-cm) posts on a flat-faced injector. Three post diameters were used.

Transverse mode. - It is readily apparent that the baffles produced significant damping for the transverse mode because of their obstructive behavior. The increase over

TABLE III. - COEFFICIENTS OF DECAY PER CYCLE K' AND RESONANT FREQUENCIES f FOR BAFFLED CONFIGURATIONS

Injector type	Mode																				
	Transverse										Longitudinal										
	Total chamber length, L_T , in. (cm)																				
	4 (10.16)		6 (15.24)		8 (20.32)		10 (25.40)		12 (30.48)		4 (10.16)		6 (15.24)		8 (20.32)		10 (25.40)		12 (30.48)		
	Nozzle convergence angle, α , deg																				
	180		180		180		26		180		180		180		180		26		180		
K'	f , cps	K'	f , cps	K'	f , cps	K'	f , cps	K'	f , cps	K'	f , cps	K'	f , cps	K'	f , cps	K'	f , cps	K'	f , cps		
Flat		0.0721	1389	0.0524	1370	0.0419	1362	0.0704	1451	0.0304	1367	0.0252	1905	0.0383	1241	0.0350	921	0.0396	770	0.1295	598
Flat with vanes		0.1251	785	0.1221	872	0.0805	881	0.1100	889	0.0980	905	0.0467	1892	0.0503	1230	0.0763	908	-----	---	0.1180	613
Flat with vanes and ring		0.2240	775	0.1139	872	0.0825	1062	0.1140	1060	0.0955	899	0.0300	1885	0.0513	1235	0.0656	926	-----	---	0.1240	621
Protruding cone		0.1497	1205	-----	---	0.1315	1262	-----	---	0.0317	1272	-----	---	-----	---	0.0700	1038	0.0575	716	0.1090	659
Protruding cone with vanes		0.2220	852	0.1722	987	0.0990	1019	0.1942	1016	0.1380	1015	-----	---	0.0606	1420	0.0649	1033	-----	---	0.0932	667
Protruding cone with vanes and ring		0.3603	810	0.2350	947	0.2100	954	0.1750	954	0.1500	951	-----	---	0.1355	1227	0.0991	987	-----	---	0.0932	672
65 Posts, 0.13 in. diam		-----	---	0.0635	1358	-----	---	-----	---	-----	---	-----	---	0.0439	1240	-----	---	-----	---	-----	---
65 Posts, 0.30 in. diam		-----	---	0.0966	1313	-----	---	-----	---	-----	---	-----	---	0.0599	1236	-----	---	-----	---	-----	---
65 Posts, 0.50 in. diam		-----	---	0.0935	1217	-----	---	-----	---	-----	---	-----	---	0.0755	1196	-----	---	-----	---	-----	---

unbaffled configurations was as much as five times for some configurations. Decay coefficients generally decreased as the unbaffled volume of chamber increased with increased total length. In general, the baffled configurations based on the protruding cone injector gave higher losses than similar configurations with the flat injector. The 26° nozzle gave slightly higher damping with baffles than might be estimated for a 180° nozzle from the general trends of the data with total chamber length. The post baffles in the 6-inch (15.24-cm) chamber gave from 20 to 85 percent higher damping than that obtained with the plain injector, but the vaned baffles gave from 115- to 350-percent increases in damping for that length.

Longitudinal mode. - There are less longitudinal mode data at shorter chamber lengths for the coned injector because the driver position was too near the pressure node, and the mode could not be driven. Thus, the trends are not as readily evident. The baffles were not oriented to obstruct the particle motion for the longitudinal mode and had less effect on the decay coefficient than for the transverse mode. Losses in short chambers were increased by baffles because of viscous dissipation over the increased surface area. The baffles protruded farther into the region of high particle velocity in the center of these short chambers. Baffling the long chambers did not increase damping and actually decreased the loss per cycle in the 12-inch (30.48-cm) chamber with the coned injector, evidently by shortening the effective length. The protruding cone injector with both radial and ring vanes was especially effective in damping the longitudinal mode in the 6-inch-long (15.24-cm) chamber, perhaps by completely destroying the one-to-one correspondence between diameter and length which is inherent in that chamber. Also, with the exception of that configuration, the damping coefficient increased with increasing effective length (decreasing frequency), as it did for the unbaffled chambers. The post injectors, giving only slight increases, were comparable to the vane injectors.

Damping mechanism of baffles. - The damping of the two fundamental modes indicates that the primary damping influence of baffles is their obstructive nature, rather than viscous losses on the increased surface area. This is apparent from their successful attenuation of the transverse modes in which gas motion would have components normal to the baffle surfaces. It is also supported by the relatively weak effect of baffles on the longitudinal mode with particle motion parallel to the major baffle surfaces. It is difficult to conceive a parameter which would characterize the obstructive nature of baffles. The parameter would have to include not only some of the physical dimensions of the baffles but also the spatial properties of the acoustic field. The latter are known only for an idealized acoustic mode. Insertion of the baffle removes any vestige of ideality which the clean chamber field exhibited. This was observed in the baffled chambers where predicted pressure nodes around the chamber circumference could not be detected. The resulting acoustic fields, while still identifiable as transverse modes by gross pressure phase measurements around the chamber, appeared to be combinations of spinning

and standing modes with a complex small-scale spatial phase relation.

For this reason no characterization could be made. Nevertheless, the data do indicate the relative increases in damping available from simple baffles and point out the necessity of tailoring baffle design to the predominant acoustic modes which can be expected in a given thrust chamber.

CONCLUSIONS

From the results of an experimental study of acoustic decay coefficients of simulated rocket combustors, the following conclusions can be drawn:

1. Considerable increases in acoustic damping were achieved by the insertion of properly designed baffles in the chambers. The damping effect was optimum when these baffles blocked the particle motion produced by the acoustic mode.
2. The decay coefficients obtained for unbaffled chambers are at least an order of magnitude higher than those predicted by an idealized viscous-loss theory.
3. Simple changes in chamber shape did not give dramatic increases in acoustic losses. Transverse mode damping per cycle increased with increasing internal area-to-volume ratio. Longitudinal mode decay rates increased as the chamber was lengthened, and nozzle losses for this mode were maximum with no taper on the chamber.

Lewis Research Center,
National Aeronautics and Space Administration,
Cleveland, Ohio, February 9, 1966.

REFERENCES

1. Cantrell, R. H.; and Hart, R. W.: Interaction Between Sound and Flow in Acoustic Cavities: Mass, Momentum, and Energy Considerations. *J. Acoust. Soc. Am.*, vol. 36, no. 4, Apr. 1964, pp. 697-706.
2. Priem, Richard J.: Combustion Process Influence on Stability. Preprint No. 28d, *A. I. Ch. E.*, 1965.
3. Crocco, Luigi; Harrje, David T.; and Reardon, Frederick H.: Transverse Combustion Instability in Liquid Propellant Rocket Motors. *ARS J.*, vol. 32, no. 3, Mar. 1962, pp. 366-373.
4. Smith, P. W., Jr.: Effects of Vent Geometry on Acoustic Losses of T-Burners. Preprint No. 64-135, *AIAA*, 1964.

5. Gordon, C. G.; and Smith, P. W., Jr.: Acoustic Losses in a Resonator with Steady Gas Flow. Rept. No. 1142, Bolt, Beranek and Newman, Inc., June 1964.
6. Priem, Richard J.: Attenuation of Tangential-Pressure Oscillations in a Liquid-Oxygen - n-Heptane Rocket Engine with Longitudinal Fins. NACA RM E56C09, 1956.
7. Sirignano, W. A.; and Strahle, W. C.: A New Concept in Rocket Engine Baffles. AIAA J., vol. 3, no. 5, May 1965, pp. 954-956.
8. Utvik, D. H.; Blackman, A. W.; and Ford, H. J.: Evaluation of Absorption Liners for Suppression of Combustion Instability in Rocket Engines. Paper No. 65-585, AIAA, 1965.
9. Watson, F. R.: Graphical Representation of the Reverberation Equation. J. Acoust. Soc. Am., vol. 1, no. 1, Oct. 1929, pp. 47-55.
10. Lambert, Robert F.: A Study of the Factors Influencing the Damping of an Acoustical Cavity Resonator. J. Acoust. Soc. Am., vol. 25, no. 6, Nov. 1953, pp. 1068-1083.
11. Smith, R. P.; and Sprenger, D. F.: Combustion Instability in Solid-Propellant Rockets. Fourth Symposium (International) on Combustion, The Williams & Wilkins Co., 1953, pp. 893-906.
12. Crocco, Luigi; and Cheng, Sin-I: Theory of Combustion Instability in Liquid Propellant Rocket Motors. Agardograph No. 8, Butterworths Sci. Pub., 1956, pp. 168-187.
13. Maslen, Stephen H.; and Moore, Franklin K.: On Strong Transverse Waves Without Shocks in a Circular Cylinder. J. Aeron. Sci., vol. 23, no. 6, June 1956, pp. 583-593.

"The aeronautical and space activities of the United States shall be conducted so as to contribute . . . to the expansion of human knowledge of phenomena in the atmosphere and space. The Administration shall provide for the widest practicable and appropriate dissemination of information concerning its activities and the results thereof."

—NATIONAL AERONAUTICS AND SPACE ACT OF 1958

NASA SCIENTIFIC AND TECHNICAL PUBLICATIONS

TECHNICAL REPORTS: Scientific and technical information considered important, complete, and a lasting contribution to existing knowledge.

TECHNICAL NOTES: Information less broad in scope but nevertheless of importance as a contribution to existing knowledge.

TECHNICAL MEMORANDUMS: Information receiving limited distribution because of preliminary data, security classification, or other reasons.

CONTRACTOR REPORTS: Technical information generated in connection with a NASA contract or grant and released under NASA auspices.

TECHNICAL TRANSLATIONS: Information published in a foreign language considered to merit NASA distribution in English.

TECHNICAL REPRINTS: Information derived from NASA activities and initially published in the form of journal articles.

SPECIAL PUBLICATIONS: Information derived from or of value to NASA activities but not necessarily reporting the results of individual NASA-programmed scientific efforts. Publications include conference proceedings, monographs, data compilations, handbooks, sourcebooks, and special bibliographies.

Details on the availability of these publications may be obtained from:

SCIENTIFIC AND TECHNICAL INFORMATION DIVISION
NATIONAL AERONAUTICS AND SPACE ADMINISTRATION
Washington, D.C. 20546